

Subjective nature of path information in quantum mechanics

Xinhe Jiang^{1,2†}, Armin Hochrainer^{1,2†}, Jaroslav Kysela^{1,2},
Manuel Erhard^{1,2}, Xuemei Gu^{1,3}, Ya Yu^{1,4}, Anton Zeilinger^{1,2*}

¹Institute for Quantum Optics and Quantum Information, Austrian Academy of Sciences, Boltzmannngasse 3, Vienna, 1090, Austria.

²Vienna Center for Quantum Science and Technology, Faculty of Physics, University of Vienna, Boltzmannngasse 5, Vienna, 1090, Austria.

³Max Planck Institute for the Science of Light, Staudtstraße 2, Erlangen, 91058, Germany.

⁴Shanghai Jiao Tong University, Dongchuan Road 800, Shanghai, 200240, China.

*Corresponding author(s). E-mail(s): anton.zeilinger@univie.ac.at;

†These authors contributed equally to this work.

Abstract

Common sense suggests that a particle must have a definite origin if its full path information is available. In quantum mechanics, the knowledge of path information is captured through the well-established duality relation between path distinguishability and interference visibility. If visibility is zero, high path distinguishability can be achieved, which enables one to determine with high predictive power where the particle originates. We investigate the complementarity between path information and interference visibility through an experiment involving three sources emitting into identical modes. Our findings challenge the classical intuition that a particle can be traced back to its origin through its trajectory when full path information is available. By grouping the crystals in different ways, we demonstrate that it is impossible to ascribe a definite physical origin to the photon pair, even if the emission probability of one individual source is zero and full path information is available. Our results shed new light on the physical interpretation of probability assignment and path information beyond

its mathematical meaning and show that the interpretation of path information in quantum mechanics is subjective.

Introduction

Bohr's complementarity principle [1] is a cornerstone in quantum mechanics, illustrating the mutual exclusivity of certain properties of a system—such as wave-like interference and particle-like path information. The particle nature is usually characterised by the ability to distinguish between the two paths and to analyse which slit the particle passed through, as famously exemplified by the double-slit interference experiment. Physically, the complementarity principle manifests itself as a question of predictability: could one consistently win with more than 50% probability by betting on the outcome of a which-path measurement? High path distinguishability enables such predictive power but eliminates interference visibility. Conversely, if interference fringes are observed with high visibility, no meaningful path information can be obtained, and path alternatives become entirely unascertainable. Quantitatively, the trade-off between path *distinguishability* (D) (which-path information) and *visibility* (V) of the interference fringes is encapsulated in the duality relation $D^2 + V^2 \leq 1$ [2–5], indicating that observation of an interference pattern and acquisition of which-path information are mutually exclusive. This duality relation has been extensively studied in two-path interferometers [6, 7].

A striking example of illustrating the duality relation is frustrated down-conversion [8], an interference phenomenon that occurs when photons are generated from two sources [9]. In this setup, photon pairs may be emitted from either crystal, and the two possibilities are aligned so that they overlap perfectly in both spatial and temporal modes. If the two sources are indistinguishable, which means that spontaneous parametric down-conversion (SPDC) photons from each source have the same

spatiotemporal modes, same frequency and bandwidth, etc., perfect interference can occur, i.e., the interference visibility can reach 1. However, if one source is blocked or misaligned, the photons' origin becomes distinguishable, and interference is lost. Frustrated down-conversion induces the idea of path identity, which has led to many striking quantum interference effects and quantum applications in recent years [10, 11]. Path distinguishability, in the context of frustrated down conversion, means information about which source produced the photon pair. If interference is reduced, complementarity allows for a more profitable bet on the outcome of a “which-source” measurement due to the increased amount of information concerning the source of the photons. Frustrated down-conversion thus provides a good platform to study the interplay between interference and which-source information.

The duality relation has also been extended to multi-path interference [12–16]. In such cases, interference between multiple alternative ways of emitting photon pairs can be observed, and these observations have consistently confirmed the duality relation between visibility and distinguishability [17, 18]. In this work, we used a frustrated SPDC system with three nonlinear crystals to explore a different aspect of the duality relation, namely, the interpretation of path information when applying the theoretical formalism to an actual experiment. This room for interpretation stems from the different ways of partitioning reality into alternatives, represented by probability amplitudes. We find that interpreting distinguishability as information about the origin of photon pairs is inconsistent in a three-crystal setup. Unlike the two-crystal case, ascribing a definite origin to a photon pair is impossible, even though full “path information” is available and no interference is observed if the two crystals are grouped together. This result arises because, while the quantum-mechanical formalism provides an unambiguous and objective description of the system, the interpretational narrative used to describe the underlying processes can be subjective.

Here, we show that there are multiple valid ways to assign probability amplitudes to the alternatives in the experiment, leading to incompatible interpretations of the results. In general, a given probability can be decomposed into alternative probability amplitudes, each of which may be non-zero, while their coherent superposition leads to a vanishing total amplitude. This implies that “which-path information” can only be meaningfully defined if the context is clarified and the relevant alternatives are explicitly specified in this context. This undermines the view that path information is a definitive and objective property of the system.

Results

Inconsistent which-path information in three-crystal interference

Considering that three nonlinear crystals are pumped with the same laser, which emits photon pairs into identical modes (Fig. 1a), the quantum state of the system can be written as [8, 19],

$$|\psi\rangle = ae^{i\phi_A}|s\rangle|i\rangle + b|s\rangle|i\rangle + ce^{i\phi_C}|s\rangle|i\rangle \quad (1)$$

where $ae^{i\phi_A}$, b , $ce^{i\phi_C}$ represent the probability amplitudes of photon pair creation at the respective crystal, $|s\rangle|i\rangle$ represents a signal and idler photon pair in the modes that can be detected, and ϕ_A , ϕ_C are the relative phase between the photons emitted from each pair of crystals. This state is consistent with the Hamiltonian-based models of the SU(1,1) interferometer [20], which are fundamentally different from those of the traditional Mach-Zehnder interferometer. In Supplementary Note 1, we show that our setup is actually a nonlinear interferometer with three processes. With this, the rate

of the emitted photon pairs can be written as

$$R(\phi_A, \phi_C) \propto |ae^{i\phi_A} + b + ce^{i\phi_C}|^2 \quad (2)$$

As stated, the amount of “which-source” information and visibility exhibit a trade-off relation due to the complementarity principle. By treating two of the three sources as a single source and applying the duality relation (the applicability of the duality relation to our setup is given in Supplementary Note 2), we show that analysing the “which-source” information and visibility from this point of view leads to a contradiction between two possible interpretations of the same experiment.

First, consider the first two nonlinear crystals (NL1 and NL2) to constitute one source labelled by S1, while NL3 constitutes a second source S2, as shown in Fig. 1b. With this treatment, the quantum state of the photon pair in equation (1) can be rewritten as

$$|\psi\rangle = [\alpha + ce^{i\phi_C}] |s\rangle|i\rangle \quad (3)$$

where $\alpha = ae^{i\phi_A} + b$ is the probability amplitude corresponding to photon pair emission by S1 and $ce^{i\phi_C}$ corresponds to an emission by S2. Thus, for a fixed relative phase ϕ_A between NL1 and NL2, defining the parameter α , the rate of emitted photons can be rewritten as

$$R(\phi_C) \propto |\alpha + ce^{i\phi_C}|^2 \quad (4)$$

Now, one can apply the duality relation between the observed visibility upon varying ϕ_C and the amount of available “which-source information”. Consider an experimental situation in which $a = b$ and $\phi_A = \pi$. It follows that $\alpha = 0$. Therefore,

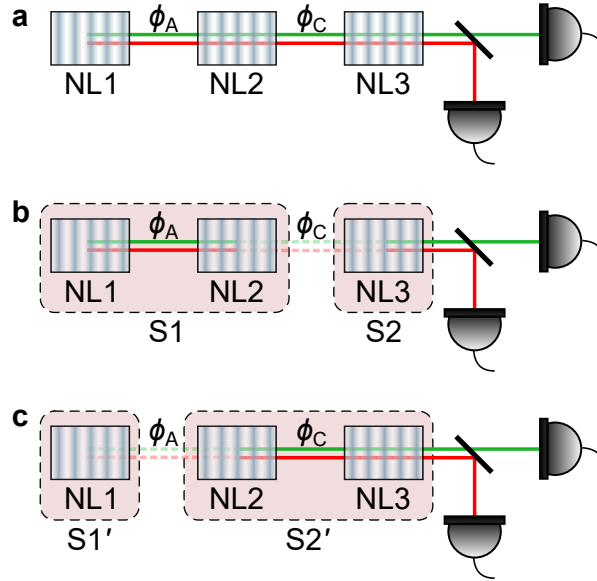


Fig. 1: Schematic of three-crystal interference. a, The three crystals emit photon pairs in identical modes. b, The combination of NL1 and NL2 is considered a single photon pair source (S1). The second source (S2) consists only of NL3. The relative phase ϕ_A between NL1 and NL2 changes the probability of S1 emission. If set to π , the photon pair emission of S1 is completely suppressed. Thus, all emitted photons come from NL3 and no visibility of the total emission rate is observed when varying the relative phase ϕ_C between S1 and S2. c, NL1 corresponds to the source S1', while the combination of NL2 and NL3 is considered a single source S2'. With the same argument, we conclude that all the photons must have originated from NL1 and no visibility is observed when varying the relative phase ϕ_A if $\phi_C = \pi$. These two contradictory situations can be realised in the same experiment when the intensities are balanced and $\phi_A = \phi_C = \pi$. Note that the phase shifter introduces a negative relative phase between NL2 and NL3. Because of its symmetry and periodicity, we represent it as ϕ_C .

the probability amplitude corresponding to a pair of photons emitted by S1 is equal to zero. Thus, S1 is “switched off”. This is consistent with the observation that S1 corresponds to a frustrated down-conversion tuned to completely destructive interference. Consequently, if S2 is removed, in principle, no pair of photons is emitted from the system. However, if instead the first “double” source (S1) is blocked or removed, the photon pair emission rate is unchanged. Therefore, there will be zero interference visibility by varying the relative phase ϕ_C between S1 and S2. These observations are consistent with the duality relation $D^2 + V^2 \leq 1$, as the sources S1 and S2 are

unbalanced and the information from “which-source” is available here. One might conclude that all photon pairs come from source S2, that is, from NL3. However, this interpretation leads to a contradiction, as is shown below.

Instead of grouping events into photon-pair emissions from S1 and S2, consider an alternative view of the experiment. Crystal NL1 is considered the first source S1' and the combination of NL2 and NL3 is considered the second source S2', as indicated in Fig. 1c. The possible events are identified accordingly as photon pair emission from either S1' or S2'. In this situation, the quantum state is

$$|\psi\rangle = [ae^{i\phi_A} + \beta] |s\rangle|i\rangle \quad (5)$$

with the probability amplitude for photon pair emission by S1' being $ae^{i\phi_A}$ and the amplitude for S2' is $\beta = b + ce^{i\phi_C}$. For a fixed relative phase ϕ_C between NL2 and NL3, defining the parameter β , the rate of emitted photons can be rewritten as

$$R(\phi_A) \propto |ae^{i\phi_A} + \beta|^2 \quad (6)$$

Similarly, we can make the following argument. Taking into account the situation where $b = c$ and $\phi_C = \pi$, it follows that $\beta = 0$. Again, the duality relation $D^2 + V^2 \leq 1$ can be applied in a self-consistent way. Individual blocking of S1' and S2' shows that S2' does not emit photon pairs. In this case, S2' is “switched off”. No interference visibility will be observed when the phase ϕ_A is varying. This corresponds to full “which-source” information. Thus, one can conclude that the photons were emitted by S1', that is, NL1.

It should be noted that both of these two situations can be realised in one experiment, allowing $a = b = c$ and $\phi_A = \phi_C = \pi$. With this setting, the corresponding rate of detected photons is non-zero and the same for these two situations through

equation (2). If we fix one phase to be π and scan another phase, this rate will remain constant, and there will be no interference visibility. At the same time, we still have no information about which crystal produced these photons. We can see that both viewpoints are equally self-consistent and obey the duality relation. However, the interpretations provided by analysing the “which-source” information in two alternative ways of partitioning the system into two separate sources are incompatible with each other.

Experimental demonstration of inconsistent which-path information

The experimental setup is shown in Fig. 2. A 405 nm pump light is used to pump the three periodically poled potassium titanyl phosphate (PPKTP) crystals. The 810 nm photon pairs (signal and idler) are generated in a collinear arrangement through a SPDC process with a type-II configuration. The three crystals emit photons into identical modes. After the third crystal, the pump light is filtered with a dichroic mirror (DM) and a band-pass filter (BPF). Finally, the SPDC photons are detected with single-photon detectors and sent to the coincidence logic for processing. The pump power is low enough so that only one photon pair at a time is present. Phase plates are placed between each pair of crystals and are used to tune the relative phase between the pump, signal, and idler photons, and thus changing the relative phase ϕ_A and ϕ_C . The lenses between each pair of crystals form a 4f system to obtain good spatial overlap of the SPDC photons from each crystal.

To obtain good interference visibility between all crystals, the spectral and spatial degrees of freedom of the SPDC photons should be indistinguishable. This can be realised with identical crystals and by overlapping their spatial mode through fine-tuning the position of lenses in the setup. To facilitate this, we used an intensified charge-coupled device (ICCD) camera to image the SPDC photons. The lens system

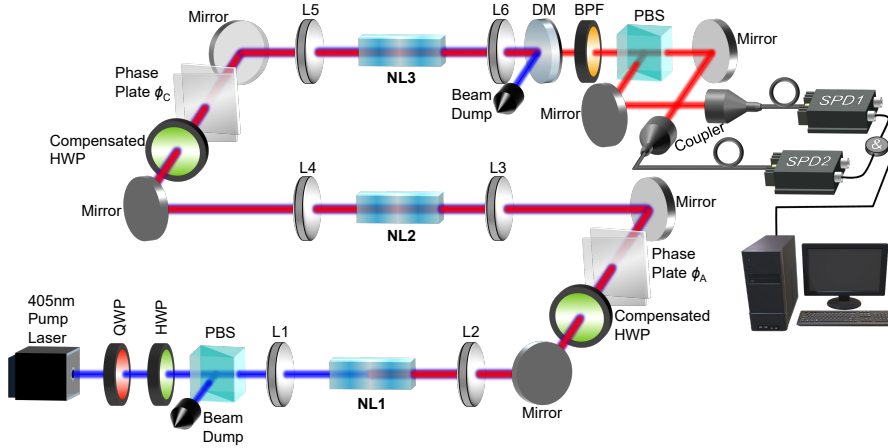


Fig. 2: Experimental setup of the three-crystal interference. The 405 nm pump laser is used to pump the three crystals. The SPDC photons are generated and emitted in identical modes. Each crystal is enclosed by two lenses, and two lenses between each pair of crystals form a 4f system. This ensures that the first crystal is imaged onto the second crystal and a good spatial overlap of the beams created in the two SPDC processes is obtained. The phase plates between each pair of crystals are used to change the relative phases (ϕ_A and ϕ_C) of the pump, signal, and idler photons. To compensate for the longitudinal walk-off caused by the different group velocities of signal and idler photons, we used two compressed half-wave plates between each pair of crystals. The photons are finally filtered and collected in the fibre for coincidence counts. QWP: quarter-wave plate. HWP: half-wave plate. PBS: polarising beam splitter. NL1-NL3: Non-linear crystals 1-3. L1-L6: lenses 1-6. DM: dichroic mirror. BPF: band-pass filter. SPD: single-photon detector. &: coincidence logic.

allows us to successively image signal and idler beams originating from each of the SPDC processes at the crystal and at its Fourier plane. The photon beams from the three SPDC processes are aligned to overlap in both planes to ensure that they are indistinguishable in any plane. The details and characteristics of the imaging are shown in the Methods, ‘Characterization of SPDC photons’. In addition, the crystal temperature is also optimised to ensure a degenerate photon pair emission from all three crystals.

To get a full view of how visibility changes when one phase is fixed and the other phase is scanned, we set different values for one phase and obtain visibility by scanning the other phase, as shown in Fig. 3. As it is periodic, only some periods are given.

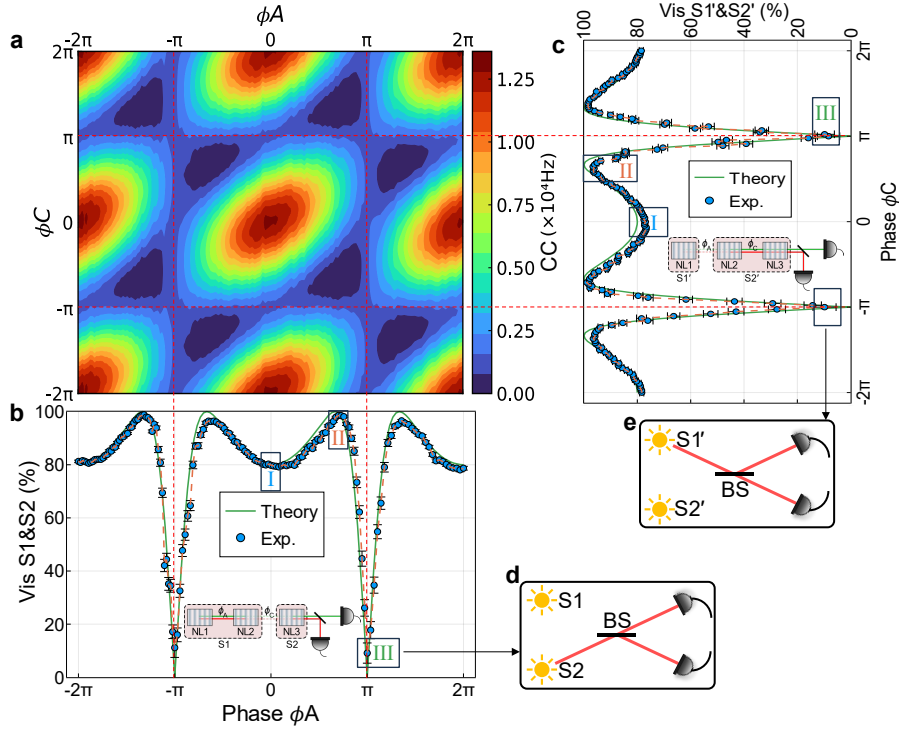


Fig. 3: Three-crystal interference obtained with a 2D scan. a, Contour plot shows the detected coincidence counts (CC) when all three crystals are active upon varying both phases ϕ_A between NL1 and NL2, and ϕ_C between NL2 and NL3. b, Visibility observed between S1 and S2 when each phase ϕ_A is fixed and phase ϕ_C is scanned. The inset shows the first perspective, which regards the system as a two-process interferometer between S1 and S2. At the phase point $\phi_A = (2k + 1)\pi$ ($k \in \mathbb{Z}$), the photon pair emission from S1 is suppressed, as shown schematically in d. c, Visibility observed between S1' and S2' when each phase ϕ_C is fixed and phase ϕ_A is scanned. The inset shows another perspective, which regards the system as a two-process interferometer between S1' and S2'. In an analogous manner, the photon pair emission from S2' is suppressed at the phase point $\phi_C = (2k + 1)\pi$ ($k \in \mathbb{Z}$), as shown schematically in e. The coincidence count data in frames I, II, III of b,c are shown in Fig. 4a,b, respectively. The green line in b and c is the theoretical prediction. The blue dot is the experimental data. The dashed orange line is a guide for the eye. BS: Beam splitter.

Figure 3a shows the contour plot when all three crystals are active and the two phases are varied. For comparison, the theoretical contour plot is given in the Supplementary Figure 3b. First, phase ϕ_A is set to different values and the visibility is calculated when phase ϕ_C is scanned (see Fig. 3b). As can be seen, visibility is highest when the

phase is set to $\phi_A = 2\pi/3$. This is because the amplitude of the combination of NL1 and NL2 is more balanced compared to the amplitude of NL3 at this point. They have better interference visibility as a result of their better indistinguishability. However, at the point $\phi_A = \pi$, they show almost no interference due to complete distinguishability. Similar results are also obtained when the phase ϕ_C is set to different values and the visibility is measured by scanning the relative phase ϕ_A (see Fig. 3c). The inset of Fig. 3b,c shows the two pictures when the crystals are grouped differently. At the phase point $(2k + 1)\pi$ ($k \in \mathbb{Z}$), the photon pair emission is suppressed, corresponding to one of the sources (S1 or S2') being switched off in the two-source interferometer, as shown schematically in Fig. 3d,e. Therefore, the knowledge that photons can only be emitted by the other source (S2 and S1') yields full interferometric path information in the sense that one could always win a bet on the outcome of the measurement on the individual sources.

In Fig. 4a,b, we plot the interference fringe at three representative phases 0, $2\pi/3$ and π , which are labelled I, II and III in Fig. 3b,c. Phase 0 has higher counts but lower visibility. Phase $2\pi/3$ has lower counts, but the highest visibility. Phase π exhibits almost no visibility. More theoretical analysis and comparison with experimental data can be found in Methods. To take a closer look at these two pictures, one of the phases is fixed as π , and the other phase is scanned. According to the theoretical analysis, we will see a constant count rate. In our experiment, the visibility of the interference between the probability amplitude contributed by S1 and that of S2 when setting $\phi_A = \pi$ is $9.12 \pm 3.81\%$. The corresponding visibility between S1' and S2' when setting $\phi_C = \pi$ is $8.30 \pm 4.19\%$. This is almost close to the random noise level when there is no interference at all. In Fig. 4c,d, we plot the coincidence counts (CC) with error bars when $\phi_A = \pi$ and $\phi_C = \pi$, respectively. It can be seen that CC fluctuates within a small range. This even reaches the random noise level. In addition, the two cases have overlapping count regions (1600-1800 Hz). In this region, we cannot tell

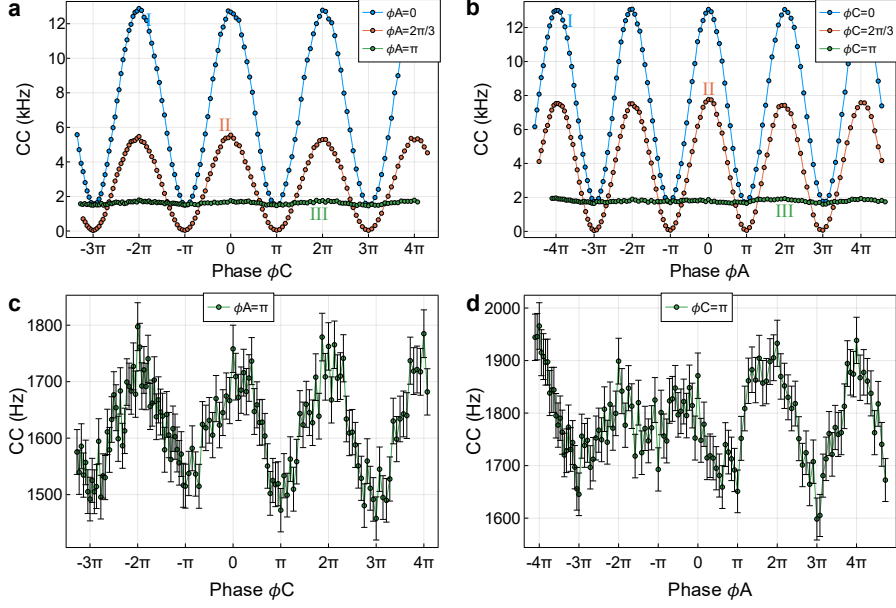


Fig. 4: Interference fringes at the phase point 0 , $2\pi/3$, and π . a,b, Coincidence counts (CC) for the three points I: $\phi_A = 0$ ($\phi_C = 0$), II: $\phi_A = 2\pi/3$ ($\phi_C = 2\pi/3$), III: $\phi_A = \pi$ ($\phi_C = \pi$) chosen in Fig. 3b,c, respectively. c, CC versus ϕ_C when relative phase $\phi_A = \pi$. d, CC versus ϕ_A when relative phase $\phi_C = \pi$. The lines are guides to the eye. Errors are determined by assuming Poissonian counting statistics.

at all from which crystal the photons come from. Using the counts data, we estimate that the path information corresponds to photon pairs originating from NL3 with the probability $p_3 = 95.14 \pm 0.59\%$ when $\phi_A = \pi$ and from NL1 with the probability $p_1 = 96.41 \pm 0.47\%$ when $\phi_C = \pi$ (probability p_1 is calculated by CC_{NL1}/CC_{tot} and probability p_3 is calculated by CC_{NL3}/CC_{tot} , where $CC_{NL1} = CC_{tot} - CC_{S2'}$ and $CC_{NL3} = CC_{tot} - CC_{S1}$, CC_{S1} and $CC_{S2'}$ are counts when the crystals NL3 and NL1 are off, respectively, and the corresponding phase ϕ_A and ϕ_C is set to π , CC_{tot} are the counts when all three crystals are on and both phases ϕ_A and ϕ_C are set to π). Using these data, the duality relation obtained in our experiment is shown in the Supplementary Table 1. As $p_1 + p_3 > 1$, we arrive at a contradiction because it is impossible to have a probability larger than 1 in an experiment carried out with $\phi_A = \phi_C = \pi$. It should be noted that it is not possible to have equal overlapping

regions and a constant count due to experimental imperfections. Therefore, visibility cannot completely become zero at phase π . The analysis of some of the experimental errors is shown in Methods, ‘Optimisation of the visibility’.

Discussion

Note that in a periodically poled crystal, the amplitudes of pair creations at different crystal sections are engineered to interfere constructively to increase the pair-creation efficiency. Usually, a single probability amplitude is assigned to photon pair emission within the whole crystal, but no description is given anymore at which position inside the crystal the photon originates. In an analogous fashion, we can also group two crystals together and assign a single probability amplitude for the photon-pair emission. However, the assignment of a probability amplitude of zero to an alternative should not be interpreted as a zero probability that this alternative will occur. In the experiment of two-crystal frustrated down-conversion [8], if one crystal emits no photons, one can determine with high probability that the detected photons originate from the second crystal. Nevertheless, the probability must include all the contributions of the three crystals if a third nonlinear crystal were inserted before the detectors. Different from the two-crystal case, a measured probability of zero for the first two crystals does not mean that no photons come from them in the presence of a third crystal, since each crystal contributes to a probability amplitude alternative, which finally interferes with each other [19].

Another interesting point is to realise the subtle difference in the operational and physical interpretation of the “which-path information” depending on what measurement is performed [19]. If the three crystals are analysed separately, “which-path information” refers to the question “which crystal generates the photons before they arrived at the detectors”. If two of them are grouped together and assigned one common probability amplitude, the “which-path information” then corresponds to the

question “which of the two possible events happened? Did the photons come from the first crystal or from a combination of the other two?” Despite these different perspectives, the amount of path information remains entirely dependent on visibility via the duality inequality. Therefore, in the situation of both phases set to π , all these pictures are equally valid and self-consistent, although they lead to incompatible which-path information.

Bohr’s complementarity principle is usually understood as the wave-particle duality relation. The visibility of an interference pattern is used to quantify the wave property, and the path information is used to quantify the particle property. The one-particle and two-particle interference are widely characterised in the framework of the duality relation. This interference phenomenon has its root in the indistinguishability of the different alternatives, which contribute to the overall quantum amplitudes of the system as a whole. In single and two-particle interferometry, this complementarity is explored through the relationship between path distinguishability and the visibility of interference fringes [2, 4, 21–23]. Compared with two-particle interference, there exist entirely different implications in three-particle interferometry that are worth further investigation [24]. Our experiment also demonstrates an important feature of quantum mechanics: the description of the interference of a system of quantum emitters (even if it is composed of spatially distinct parts in a laboratory) must encompass all possible alternatives according to the sum of the corresponding amplitudes, as long as no intervention is made to make these alternatives distinguishable. Whether the three-crystal system should be treated as a whole or can be analysed separately depends on whether their contributions to these different alternatives can be distinguished or not. This point of view may renovate our understanding of the interplay between whole and part in the context of distinguishability.

We note that some theoretical works have provided a general framework to derive wave-particle duality relations (WPDRs) based on entropic uncertainty relations

(EURs) [25]. The equivalence of WPDR and EUR has also been demonstrated in a recent experiment for two-path interferometers [26]. In the entropic view, visibility and distinguishability can be defined through some kind of entropy, which quantifies the information of the particle and wave behaviour obtained in the system. The extended framework for formulating the WPDR from EUR in multi-path interferometers [27] provides experimental insights into investigating the WPDR and its equivalence to EUR in higher dimensions, based on our current setup. This may be the subject of our follow-up work.

In this work, we showed that both no which-path information and no interference could be realised in a single experiment by involving three indistinguishable sources. By treating two of the three sources as a single source, two incompatible interpretations of the path information are possible within a single experimental configuration. This brings about a refinement of the physical interpretation and experimental description of “which-path information”. Usually, we identify macroscopically distinguishable “alternatives” and assign probability amplitudes to them. However, this identification of “alternatives” is generally ambiguous. Our findings suggest that path information depends not only on the physical system, but also on how to translate the formula to an actual experiment. This offers a fresh perspective on quantum interference. By revealing the subtleties of frustrated down-conversion in multi-crystal setups, this work deepens our understanding of quantum phenomena and raises important questions about the nature of path information in quantum mechanics.

Methods

Theoretical analysis

In this section, we present more theoretical results of the three-crystal interference. As stated in the main text, the rate of the emitted photon pairs can be calculated through the equation (2).

Assuming that the three crystals emit photons with the same amplitude, that is, $a = b = c = 1$, the count rate can be obtained when varying the two phases. The count rate versus the phases ϕ_A and ϕ_C is shown in Supplementary Figure 3. Note that at the point $\phi_A = \phi_C = \pi$, there is a non-zero photon pair emission rate with zero visibility.

The cross-section for different phases ϕ_A is shown in the Supplementary Figure 4. Due to symmetry, the result is the same for phase ϕ_C . We choose several representative points to see how the visibility changes with the phases. We can see that the visibility is highest at the point $2\pi/3$ and becomes zero at the point π . The counts of $\pi/3$ ($2\pi/3$) and $5\pi/3$ ($4\pi/3$) are symmetric with respect to $\phi = \pi$. Therefore, they show the same visibility. To compare them, the minimum (maximum) point of the experimental data is aligned at π ($2\pi/3$) in the main text (Fig. 3). Due to periodicity, the two points $\phi_A = 0$ and $\phi_A = 2\pi$ overlap each other. One feature is that the minimal and maximal counts at the middle phase point (e.g. $\phi_A = \pi/3$) are higher than at the lowest visibility point (i.e. $\phi_A = \pi$). To provide a comprehensive comparison, we again show the visibility over the period from -2π to 2π in Supplementary Figure 5. Theoretically, the visibility is 0 at phase π and 1 at phase $2\pi/3$. The visibility is 80% when the relative phase is 0.

Characterization of SPDC photons

To guarantee that the SPDC photons from the three crystals have a good spatial overlap, we placed crystals one by one and imaged the SPDC photons with an ICCD camera. The setup of the imaging system is shown in the Supplementary Figure 6. This system allows for successive images of both SPDC processes at the crystal and at its Fourier plane. Without L7 in place, the lenses L2, L3, and L6 map the Fourier plane of the crystals to the camera plane. If the lens L7 is inserted, the two lenses after each crystal make up an imaging system that produces an image of the crystal in the camera. Therefore, the photons from the SPDC processes of each crystal are aligned

to overlap in both planes, which ensures their indistinguishability in any plane. After this alignment, the lens system and camera are removed from the setup using a flip mirror (FM). The images of the SPDC photons from the three crystals are shown in Supplementary Figure 7. We can see that they are almost the same size at both the Fourier plane and the crystal plane after good alignment.

The interference visibility between each pair of crystals is first optimised in the experiment. The results are shown in Supplementary Figure 8. The visibility is quantified by $\text{Vis} = (CC_{\text{Max}} - CC_{\text{Min}})/(CC_{\text{Max}} + CC_{\text{Min}})$, where CC is the coincidence count rate. After recursive optimisation, the observed visibility between NL1 and NL2 is $V_{12}=98.53 \pm 0.18\%$ and the visibility between NL2 and NL3 is $V_{23}=98.68 \pm 0.17\%$. For the source pair NL1&NL2 and NL2&NL3, the count rates can be expressed as in the non-ideal interference,

$$\begin{aligned} R_{12}(\phi) &= A^2 + B^2 + 2AB \cdot \cos e1 \cdot \cos \phi \\ R_{23}(\phi) &= B^2 + C^2 + 2BC \cdot \cos e3 \cdot \cos \phi \end{aligned} \quad (7)$$

A , B and C are amplitudes corresponding to each crystal, $e1$ and $e3$ accounts for the degree of coherence in the non-ideal case. Defining $s1 = A(\cos e1|1, 0, 0\rangle + \sin e1|0, 1, 0\rangle)$, $s2 = B|1, 0, 0\rangle$, $s3 = C(\cos e3|1, 0, 0\rangle + \sin e3|0, 0, 1\rangle)$ in the three-mode Fock space $|1, 0, 0\rangle$, $|0, 1, 0\rangle$, $|0, 0, 1\rangle$, the quantum state can be constructed as,

$$|\psi\rangle = s1 + s2 \cdot e^{i\phi_1} + s3 \cdot e^{i(\phi_1+\phi_2)} \quad (8)$$

Then, using the number operator $\hat{n} = \hat{a}^\dagger \hat{a}$, one can estimate the visibility between NL1 and NL3 without NL2, i.e., $s2=0$, and assuming $\phi_1=0$ without loss of generality. Based on the measured counts and visibility V_{12} and V_{23} , the estimated visibility of NL1 and NL3 is $V_{13}=97.24 \pm 0.25\%$. This indicates that each pair of crystals exhibits a high degree of coherence.

Note that the spectral and spatial distributions of the SPDC photons from the PPKTP crystal are correlated. Both are influenced by the pump wavelength, the bandwidth of the band-pass filter, and the crystal temperature. To graphically illustrate the phenomena, we schematically plot the angle distribution of the SPDC photons versus the wavelength at different crystal temperatures, as shown in Supplementary Figure 9a. The filter for different bandwidths is also plotted. One observation is that the SPDC photons appear to be located in a ring when the temperature is low. It then becomes a spot as the temperature increases. The narrower the bandwidth of the filter, the higher the temperature it needs for the photons at the centre to appear. The image measured with the temperature change is shown in Supplementary Figure 9b-g. These results are consistent with previous work [28]. Usually, we need to adjust the temperature at which the SPDC photons at 0° just appear within the bandwidth, for example, the curve of temperature T_3 in Supplementary Figure 9a. This can ensure that the photons have a good collinear overlap. The intersection point of the H and V photons is the degenerate point, which is at the double of the pump wavelength. In the experiment, it is hard to adjust the central wavelength of the band-pass filter and the degenerate point to be the same. This will cause asymmetry of the H and V photons. When the H- and V-photons exchange the roles with the compensated HWP between each pair of crystals, the photons from the two crystals will have some distinguishability because of this asymmetry. This is one of the sources of errors that cause visibility degradation.

Comparison of experimental and theoretical data

In the main text, we compare the experimental and theoretical visibility for the 2D scan. Here, we calculate the theoretical counts when one phase is fixed and the other phase is scanned, and compare it with our experimental data. For simplicity, we pick up three representative points, that is, 0 , $2\pi/3$, and π . The counts versus the phase are

shown in the Supplementary Figure 10. We can see that the visibility at phase $2\pi/3$ is the highest, i.e., 1 in theory. The visibility at phase π is 0 in theory. The visibility at phase 0 is 80% in theory. Our experimental data are in good agreement with the prediction of the theory.

Optimisation of the visibility

In the experiment, the SPDC photons must have a good spatial and spectral overlap to have a good indistinguishability. The spatial overlap can be easily realised by imaging the photons and adjusting the lens system and the translation and tilt of the crystals. To have a good spectral overlap, we use a band-pass filter. Some unwanted photons, which cause the distinguishability, can also be filtered with a single-mode fibre. In addition, the crystal temperature also needs to be optimised back and forth. To ensure coherent emission of these crystals, the optical path-length difference (OPLD) should also meet some requirements. One is that the OPLD between the pump beam and the two down-converted photons must be smaller than the coherence length of the pump laser [10],

$$|(L_{P_i} + L_{SPDC_i}) - (L_{P_j} + L_{SPDC_j})| \underset{(i,j) \in \{1,2,3\}}{\overset{i \neq j}{\leq}} L_P^{\text{coh}} \quad (9)$$

where $L_{P_{i/j}}$ are the optical path length of the pump beam from the pump laser to each crystal, $L_{SPDC_{i/j}}$ represent the optical path length of the respective down-converted photons from each crystal to the detector, and L_P^{coh} denotes the coherence length of the pump laser. Another condition is that the OPLD of the down-converted photons should be less than their coherence length,

$$|(L_{S_j} - L_{I_j}) - (L_{S_i} - L_{I_i})| \underset{(i,j) \in \{1,2,3\}}{\overset{i \neq j}{\leq}} L_{SPDC}^{\text{coh}} \quad (10)$$

with $L_{S_{i/j}}$ representing the optical path length of the signal photons from each crystal to the detector and $L_{I_{i/j}}$ for idler photons, $L_{\text{SPDC}}^{\text{coh}}$ denoting the coherence length of the down-converted photons. The first condition is easy to fulfill. To fulfill the second condition, we placed a compensated half-wave plate in the path. This wave plate is used to exchange the polarisation of the signal and idler photons and to compensate for the longitudinal walk-off between them. This will make their OPLD within the coherence length of the down-converted photons.

The general procedure of optimisation is first to adjust the coupling to get the maximal coincidence counts from the first crystal. The second crystal then opens. The SPDC efficiency is adjusted by tilting and moving the position of the crystal. The purpose is to make the counts of the two crystals as equal as possible. Then the phase between the two crystals is scanned. The temperature of the crystals is tuned to maximise their interference visibility. In addition, the relative position of the two crystals is tuned to further improve visibility. The third crystal is opened after a good visibility for the first two crystals is obtained. Meanwhile, the first crystal is closed. Then, the position and temperature of the third crystal are optimised to maximise the visibility of the last two crystals. To keep the visibility of the first two crystals, the second crystal is not touched. After good visibility is obtained, we return to the first two crystals. The second crystal is adjusted to ensure that both pairs have good visibility. This procedure is repeated many times until we get good visibility on both sides. The phase is very sensitive to air fluctuations and mechanical vibration. To stabilise the phase, we isolate the setup with a box. After this, we can do a 2D scan in the long run.

One thing is that visibility degrades over time. This is caused by some residual strain on the mount stages of each optical component. Note that any small disturbance can induce a change in the spatial position of the SPDC beams and thus lead to

the distinguishability of the SPDC photons from each crystal. Based on the theoretical model, all the errors that degrade visibility can be ascribed to three cases, namely the longitudinal misalignment, the transversal misalignment, and the tilt of each optical component. We have an estimation of these errors using relation $V^2 + D^2 = 1$ and define the quantity D as any non-overlap portion of the beam which leads to the distinguishability. The visibility degradation caused by these errors is shown in Supplementary Figure 11. The transversal and tilt errors have the most important influence on the visibility. Because the beam size is focused at about $50 \mu m$, any transversal deviation at this scale will cause a great reduction in visibility. The tilt error will be magnified with the propagation distance. As shown in Supplementary Figure 11a, the two beams overlap at position 1 and deviate from each other with a tilt angle θ . After distance L , they are fully distinguishable. With a realistic propagation distance of 400 mm between the two crystals, we get the variation of visibility versus the tilt angle. For our setup, the beams propagate longer distances before they are collected in the fiber. A 0.1° tilt will reduce visibility to 97%. Therefore, we must carefully optimise the position and tilt of each optical component and crystal.

Another factor that influences visibility is the photon yield imbalance. This is because the pump power in each crystal cannot be the same due to the non-unity transmission of the optical components between the crystals. Assume that the photon yields of NL1, NL2, and NL3 are A , B , and C , respectively. The ideal case is $B/A = 1$ and $C/A = 1$. We theoretically analyse the photon yield imbalance error, which is shown in Supplementary Figure 12. We can see that the error has a significant influence on the phase points of π and 0. With an imbalance of 0.9, the visibility at phase π has already deviated from the ideal value of 0 to 10%. Based on our measurements, the photon yields are approximately $A = 2200$ Hz, $B = 2000$ Hz, and $C = 1800$ Hz for each crystal. By substituting these experimental values, our visibility shows good agreement with the theoretical results taking these realistic errors into account.

Data availability

The data that support the findings of this study are available within the main text and its Supplementary Information. Source data are provided with this paper.

Code availability

The code used for data analysis is available from the corresponding authors upon reasonable request.

References

- [1] Bohr, N. The quantum postulate and the recent development of atomic theory. *Nature* **121**, 580–590 (1928).
- [2] Greenberger, D. M. & Yasin, A. Simultaneous wave and particle knowledge in a neutron interferometer. *Phys. Lett. A* **128**, 391–394 (1988).
- [3] Herzog, T. J., Kwiat, P. G., Weinfurter, H. & Zeilinger, A. Complementarity and the quantum eraser. *Phys. Rev. Lett.* **75**, 3034–3037 (1995).
- [4] Jaeger, G., Shimony, A. & Vaidman, L. Two interferometric complementarities. *Phys. Rev. A* **51**, 54–67 (1995).
- [5] Englert, B.-G. Fringe visibility and which-way information: An inequality. *Phys. Rev. Lett.* **77**, 2154–2157 (1996).
- [6] Dürr, S., Nonn, T. & Rempe, G. Fringe visibility and which-way information in an atom interferometer. *Phys. Rev. Lett.* **81**, 5705–5709 (1998).
- [7] Abranyos, Y., Jakob, M. & Bergou, J. Interference and partial which-way information: A quantitative test of duality in two-atom resonance. *Phys. Rev. A* **61**,

013804 (1999).

- [8] Herzog, T. J., Rarity, J. G., Weinfurter, H. & Zeilinger, A. Frustrated two-photon creation via interference. *Phys. Rev. Lett.* **72**, 629–632 (1994).
- [9] Pfleegor, R. L. & Mandel, L. Interference of independent photon beams. *Phys. Rev.* **159**, 1084–1088 (1967).
- [10] Hochrainer, A., Lahiri, M., Erhard, M., Krenn, M. & Zeilinger, A. Quantum indistinguishability by path identity and with undetected photons. *Rev. Mod. Phys.* **94**, 025007 (2022).
- [11] Krenn, M., Hochrainer, A., Lahiri, M. & Zeilinger, A. Entanglement by path identity. *Phys. Rev. Lett.* **118**, 080401 (2017).
- [12] Dürr, S. Quantitative wave-particle duality in multibeam interferometers. *Phys. Rev. A* **64**, 042113 (2001).
- [13] Zawisky, M., Baron, M. & Loidl, R. Three-beam interference and which-way information in neutron interferometry. *Phys. Rev. A* **66**, 063608 (2002).
- [14] Bimonte, G. & Musto, R. On interferometric duality in multibeam experiments. *Journal of Physics A: Mathematical and General* **36**, 11481 (2003).
- [15] Englert, B.-G., Kaszlikowski, D., Kwek, L. C. & Chee, W. H. Wave-particle duality in multi-path interferometers: General concepts and three-path interferometers. *Int. J. Quantum Inf.* **06**, 129–157 (2008).
- [16] Asad Siddiqui, M. & Qureshi, T. Three-slit interference: A duality relation. *Progress of Theoretical and Experimental Physics* **2015**, 083A02 (2015).

- [17] Heuer, A., Menzel, R. & Milonni, P. W. Complementarity in biphoton generation with stimulated or induced coherence. *Phys. Rev. A* **92**, 033834 (2015).
- [18] Heuer, A., Menzel, R. & Milonni, P. W. Induced coherence, vacuum fields, and complementarity in biphoton generation. *Phys. Rev. Lett.* **114**, 053601 (2015).
- [19] Hochrainer, A. *Path Indistinguishability in Photon Pair Emission*. Ph.D. thesis, University of Vienna (2020).
- [20] Volkoff, T. J. Relative phase and dynamical phase sensing in a hamiltonian model of the optical su(1,1) interferometer (2025). [2505.15635](#).
- [21] Horne, M. A., Shimony, A. & Zeilinger, A. Two-particle interferometry. *Phys. Rev. Lett.* **62**, 2209–2212 (1989).
- [22] Jaeger, G., Horne, M. A. & Shimony, A. Complementarity of one-particle and two-particle interference. *Phys. Rev. A* **48**, 1023–1027 (1993).
- [23] Abouraddy, A. F., Nasr, M. B., Saleh, B. E. A., Sergienko, A. V. & Teich, M. C. Demonstration of the complementarity of one- and two-photon interference. *Phys. Rev. A* **63**, 063803 (2001).
- [24] Greenberger, D. M., Horne, M. A. & Zeilinger, A. Multiparticle Interferometry and the Superposition Principle. *Phys. Today* **46**, 22–29 (1993).
- [25] Coles, P. J., Kaniewski, J. & Wehner, S. Equivalence of wave–particle duality to entropic uncertainty. *Nature Commun.* **5**, 5814 (2014).
- [26] Spegel-Lexne, D. *et al.* Experimental demonstration of the equivalence of entropic uncertainty with wave-particle duality. *Sci. Adv.* **10**, eadr2007 (2024).

- [27] Coles, P. J. Entropic framework for wave-particle duality in multipath interferometers. *Physical Review A* **93**, 062111 (2016).
- [28] Lee, S. M., Kim, H., Cha, M. & Moon, H. S. Polarization-entangled photon-pair source obtained via type-ii non-collinear spdc process with ppktp crystal. *Opt. Express* **24**, 2941–2953 (2016).
- [29] Yurke, B., McCall, S. L. & Klauder, J. R. $Su(2)$ and $su(1,1)$ interferometers. *Phys. Rev. A* **33**, 4033–4054 (1986).

Acknowledgements

We thank R. Kindler for many helpful discussions. This work was supported by the Austrian Academy of Sciences, the European Research Council [SIQS, Grant 600645 EU-FP7-ICT], the Austrian Science Fund (FWF) [FoQuS, grant-DOI 10.55776/F40 and CoQuS, Grant-DOI 10.55776/W1210], and the University of Vienna [Quantum Experiments on Space Scale, QUESS]. The authors have applied a CC BY public copyright license to any author accepted manuscript version arising from this submission.

Author contributions

X. J., A. H., J. K. and M. E. carried out the experiment. X. J. collected the data with assistance from J. K., X. G. and Y. Y.. X. J. and A. H. analysed the data and performed the numerical calculations. X. J. wrote the paper with the input of all other authors. A. H. and A. Z. conceived the project. A. Z. supervised the research. All authors discussed the experimental results.

Competing interests

The authors declare no competing interests.

Supplementary Information for “Subjective nature of path information in quantum mechanics”

Xinhe Jiang^{1,2†}, Armin Hochrainer^{1,2†}, Jaroslav Kysela^{1,2},
Manuel Erhard^{1,2}, Xuemei Gu^{1,3}, Ya Yu^{1,4}, Anton Zeilinger^{1,2*}

¹Institute for Quantum Optics and Quantum Information, Austrian
Academy of Sciences, Boltzmannngasse 3, Vienna, 1090, Austria.

²Vienna Center for Quantum Science and Technology, Faculty of
Physics, University of Vienna, Boltzmannngasse 5, Vienna, 1090, Austria.

³Max Plank Institute for the Science of Light, Staudtstraße 2, Erlangen,
91058, Germany.

⁴Shanghai Jiao Tong University, Dongchuan Road 800, Shanghai,
200240, China.

*Corresponding author(s). E-mail(s): anton.zeilinger@univie.ac.at;

†These authors contributed equally to this work.

Contents

Supplementary Notes 1-2

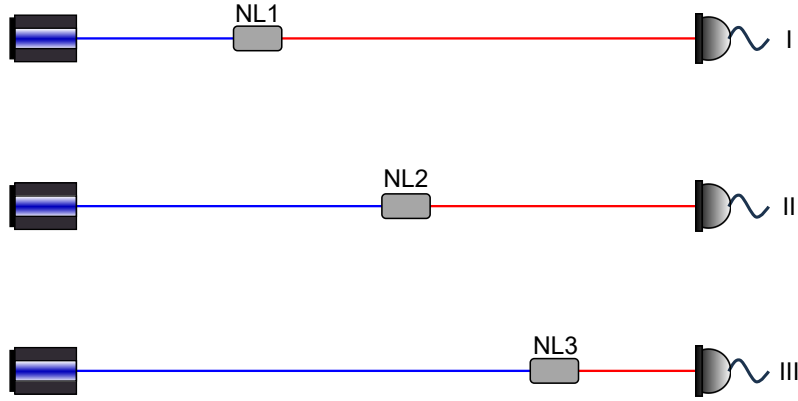
Supplementary Figures 1-12

Supplementary Table 1

Supplementary Note 1: Interference of three processes

In this section, we show that our setup is a nonlinear interferometer with three processes, and the interpretation of path information is indeed subjective. The nonlinear interferometer incorporates a $SU(1,1)$ transformation and is fundamentally different from the traditional $SU(2)$ Mach-Zehnder and Hong-Ou-Mandel-type interferometer [29]. It describes an *active* optical dynamics, which means that the ports of the interferometer can be left in vacuum. Therefore, one can treat our setup as three alternative processes that occur within each crystal as a result of second-harmonic generation. In Supplementary Figure 1, we plot the three processes. The first process I is from the pump laser to crystal NL1 and to the detector. The second process II is from the pump laser to the crystal NL2 and to the detector. The third process III is from the pump laser to the crystal NL3 and to the detector. Each crystal contributes to an alternative, that is, NL1 to $A = ae^{i\phi_A}|s\rangle|i\rangle$, NL2 to $B = b|s\rangle|i\rangle$, and NL3 to $C = ce^{i\phi_C}|s\rangle|i\rangle$. When treating the system as a whole, one accounts for all these terms and interprets the probability as $P_{\text{three}} = |A + B + C|^2$.

In the case of two-crystals (NL1 contributes to $A = ae^{i\phi_A}|s\rangle|i\rangle$, NL2 contributes to $B = b|s\rangle|i\rangle$), one has $P_{\text{two}} = |A + B|^2$. Assuming $A = 0$, we have $P_{\text{two}} = |0 + B|^2 = CC$. An experimenter is asked to determine the origin of the detected photons. The experimenter can perform the experiment. They first remove NL1 or filter the SPDC photons from NL1 and find that the detectors have counts CC . Then, they move NL1 in or remove the filter and find that the counts are still the same. The experimenter also operates NL2 in the same way. They will find that the counts are zero when NL2 is removed and that the counts remain CC when NL2 is present. Thus, the experimenter concludes that the photons originate from NL2. This is in accordance with the mathematical meaning. Therefore, one can have a high probability



Supplementary Figure 1: Interference of three processes. The first process I is from the pump laser to NL1 and to the detector. The second process II is from pump laser to NL2 and to the detector. The third process III is from the pump laser to NL3 and to the detector. Each crystal contributes to one interference term, i.e., NL1 to $A = ae^{i\phi_A}|s\rangle|i\rangle$, NL2 to $B = b|s\rangle|i\rangle$, and NL3 to $C = ce^{i\phi_C}|s\rangle|i\rangle$.

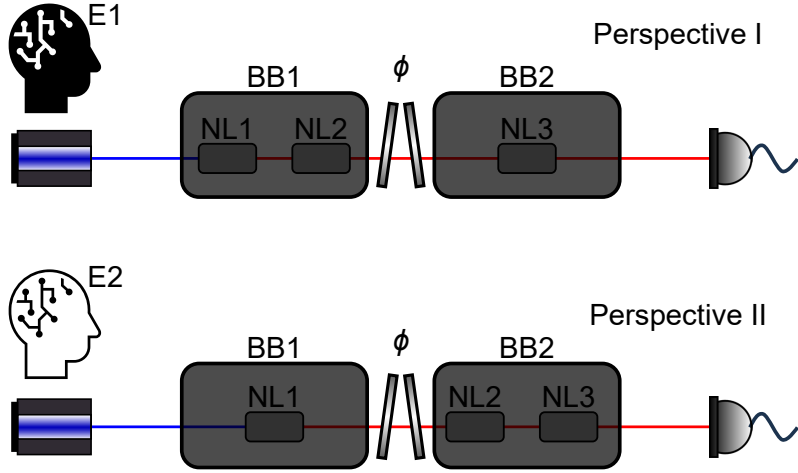
of knowing where the photons come from if one source emits no photons in the two-crystal case. The mathematical meaning and the final physical interpretation, based on the observation of the experimenter, are consistent.

In the three-crystal case, different experimenters can arrive at different conclusions for the same underlying setup. Conceiving the Gedankenexperiment (see Supplementary Figure 2): Two experimenters (E1 and E2) receive a setup composed of two black boxes (BB1, BB2), and a phase shifter is inserted between these two boxes. For E1, NL1&NL2 is placed into BB1 and NL3 is in BB2. No photons are emitted from NL1&NL2. For E2, NL1 is placed into BB1 and NL2&NL3 is in BB2. No photons are emitted from NL2&NL3. Similarly, the experimenters are asked to determine the origin of the photons. Based on their experience in the two-crystal case, the experimenters can perform a similar operation by treating each black box as a source. First, they remove BB1 and then reinsert it; second, they remove BB2 and then reinsert it. After this, experimenter E1 comes to the conclusion that under these observations, the probability amplitude for photon-pair generation in crystals NL1&NL2 does not contribute to the detected events. Consequently, conditioned on detection, the

photon pairs can be operationally attributed to crystal BB2=NL3. Whereas experimenter E2 concludes that the photons can be attributed to crystal BB1=NL1 based on their observation. One sees that fundamentally both experimenters have the same experimental setup. The different conclusions they obtained are simply because they conceptualize the experiment differently, or the experimental setup manifests itself differently. These two perspectives just correspond to the two different mathematical possibilities, i.e., $P_{\text{three}}^{(1)} = |0 + C|^2$ and $P_{\text{three}}^{(2)} = |A + 0|^2$, if $\phi_A = \phi_C = \pi$ and $|A|^2 = |B|^2 = |C|^2$. Here, one can see that interpretations of path information are highly subjective. It depends on how one conceptualizes the experiment's configuration. Furthermore, if a third experimenter finds that one black box has two crystals and opens the black boxes, they will interpret that all three crystals contribute to the counts if they are quantum physicists and believe in quantum rules. Or, in an ingenious way, they can say that the photons come from the system as a whole. In the case of two crystals, there is no inconsistency in the interpretation of the path information. The inconsistency and subjectivity in the interpretation of path information emerge only in the three-crystal case.

Supplementary Note 2: Apply duality relation in our setup

Here we show that the duality relation can be applied directly to our setup. For interferometry with two crystals, the photon pair emission rate is described by an interference law analogous to the two-path interferometer, i.e., $R \propto |a + e^{i\phi}b|^2 \propto a^2 + b^2 + 2ab \cos \phi$, where a and $e^{i\phi}b$ are the corresponding probability amplitudes contributed by these two crystals, and ϕ is the relative phase between these amplitudes. To apply the duality relation to our setup, we define the interference visibility V



Supplementary Figure 2: Two perspectives to interpret the experiment. Perspective I: NL1&NL2 is placed into black box 1 (BB1) and NL3 is placed into BB2, and no photon is emitted from NL1&NL2. Perspective II: NL1 is placed into BB1 and NL2&NL3 is placed into BB2, and no photon is emitted from NL2&NL3. Each experimenter performs the following experiment: They first remove BB1 and then reinsert it; secondly, they remove BB2 and then reinsert it. E1: Experimenter 1. E2: Experimenter 2.

similar to the traditional two-path interferometer

$$V = \frac{R_{\max} - R_{\min}}{R_{\max} + R_{\min}} = \frac{2ab}{a^2 + b^2} \quad (11)$$

The distinguishability D in this case corresponds to the distinguishability of “which-source” produced a photon pair, and can be quantified in a similar way as in the traditional two-path interferometer [2]

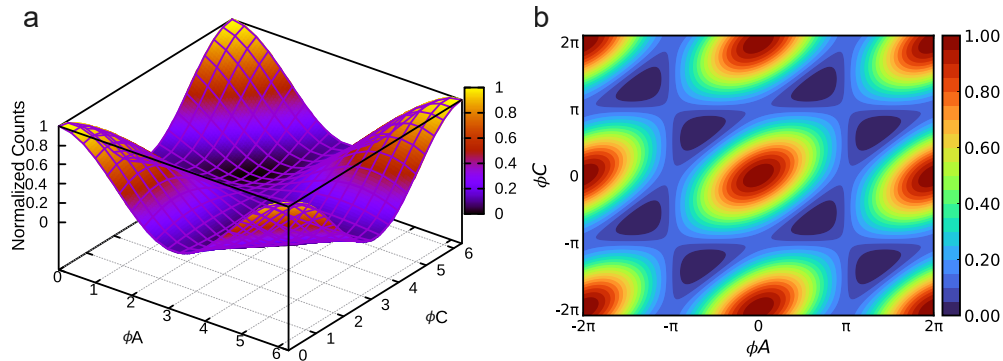
$$D = \frac{a^2 - b^2}{a^2 + b^2} \quad (12)$$

With this, the duality relation can be directly used in our setup. The “which-source” information is simply that the photon pair is produced at which source and travels all

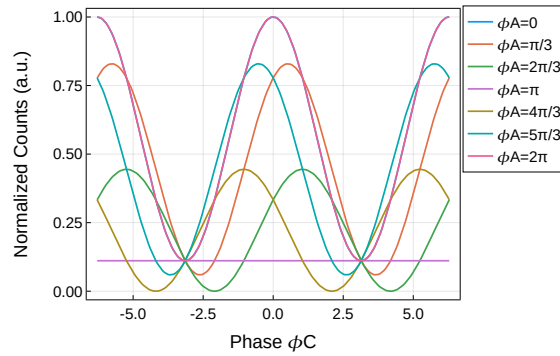
the way to the detector. When full path information is available, it means that one knows where the photon pair originated.

Supplementary Table 1: Experimentally obtained duality relations.

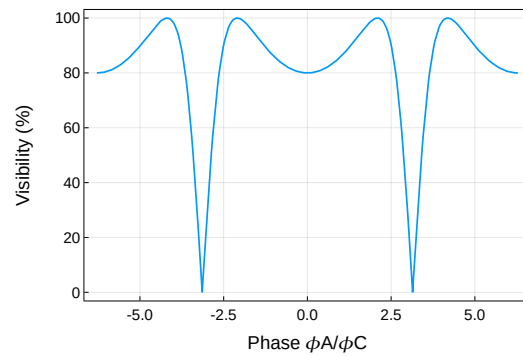
	V	$D = p3^2/p1^2$	V^2	D^2	$D^2 + V^2$
S1&S2	0.0912	0.9514	0.008317	0.905162	0.913479
S1'&S2'	0.0830	0.9641	0.006889	0.929489	0.936378



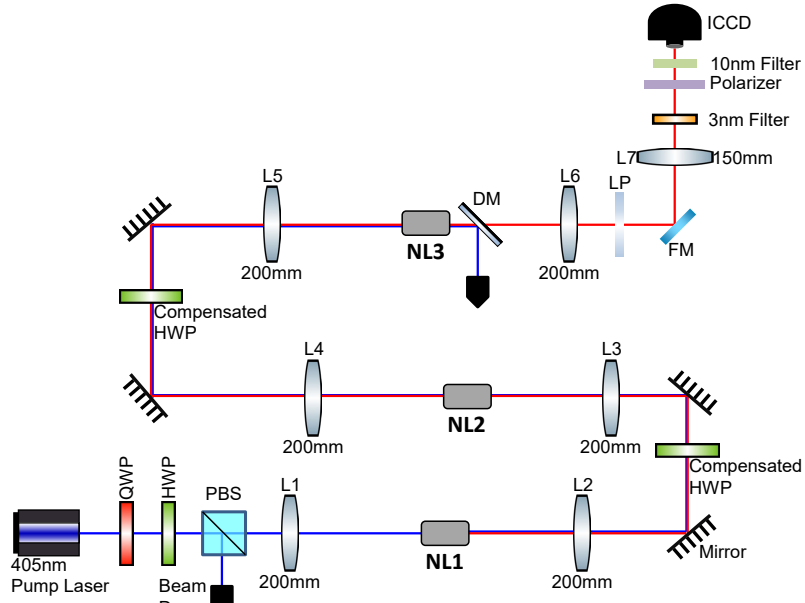
Supplementary Figure 3: a, Count rates on varying phase ϕ_A and ϕ_C obtained with equation (2) in the main text. The range is from 0 to 2π . b, Theoretical contour plot in the range from -2π to 2π . Equal emission probabilities a , b , and c are assumed. At the point $\phi_A = \pi$ or $\phi_C = \pi$, one can see that interference visibility is zero.



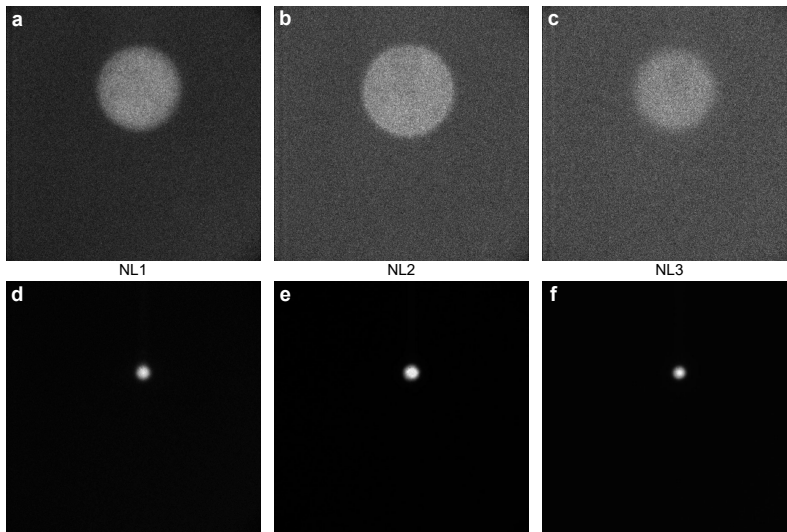
Supplementary Figure 4: Count rates versus phase ϕ_C for several fixed phases $\phi_A = 0, \pi/3, 2\pi/3, \pi, 4\pi/3, 5\pi/3, 2\pi$. Note that the highest visibility curve has a lower count rate and the middle visibility curve has a higher count rate.



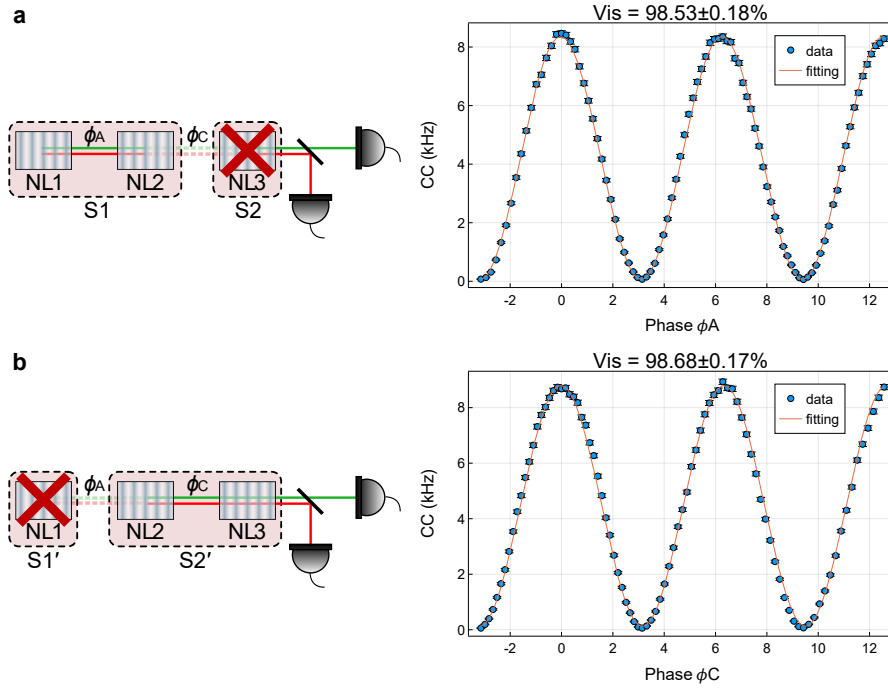
Supplementary Figure 5: Interference visibility between the three crystals. The range is from -2π to 2π . Three particular points are interesting for us to compare, i.e., phase 0, phase $2\pi/3$ of highest visibility 1, and phase π of zero visibility.



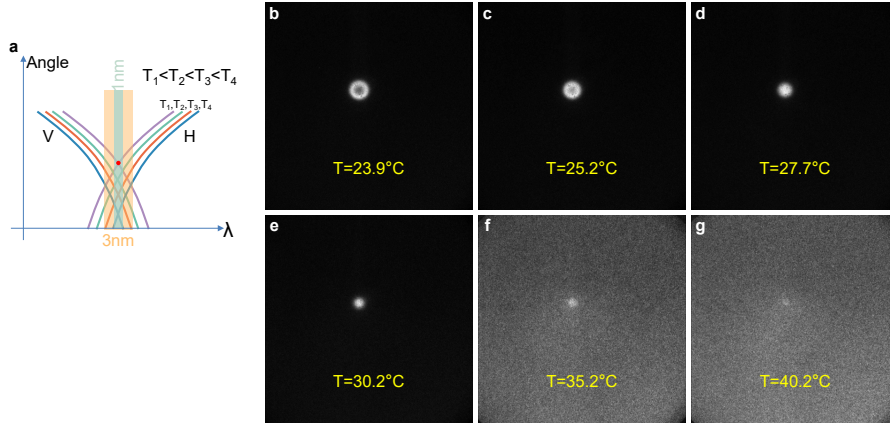
Supplementary Figure 6: Setup for the imaging of the SPDC photons from the three crystals. The setup before the flop mirror (FM) is almost the same as in the main text; only the phase plate is not included. After FM, we used an imaging system to image the SPDC photons on the ICCD camera.



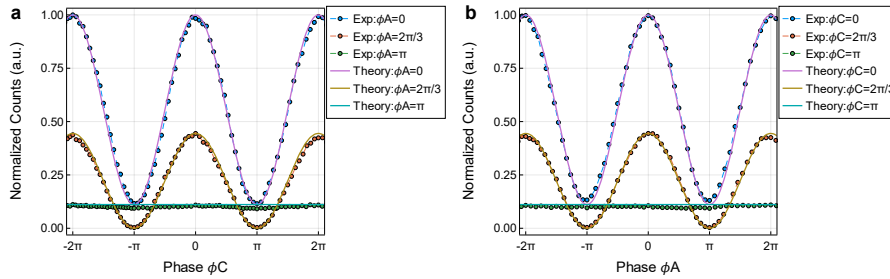
Supplementary Figure 7: Image of the SPDC photons from the three crystals with an ICCD camera. a-c are for the Fourier plane. d-f are for the crystal plane.



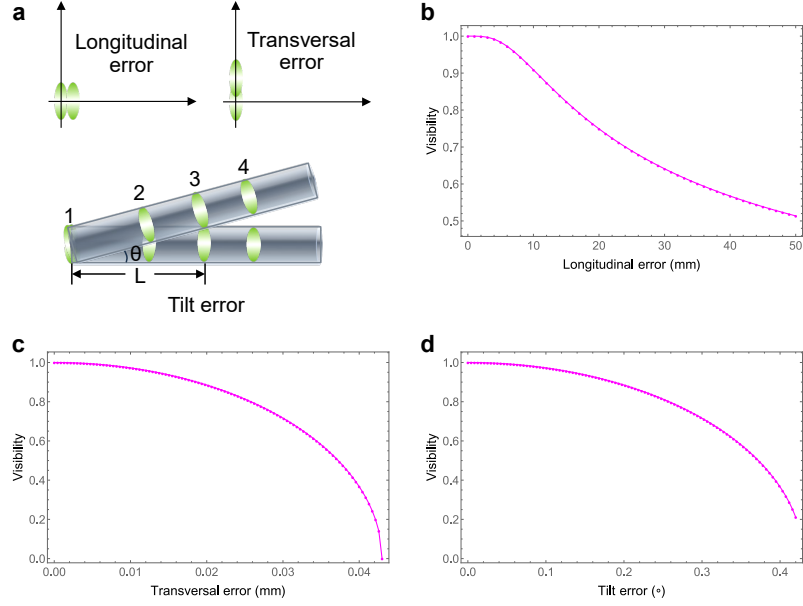
Supplementary Figure 8: Interference between each pair of crystals. a, Left: Grouping of NL1 and NL2. Right: Coincidence counts (CC) versus relative phase ϕ_A when NL3 is blocked. The interference visibility obtained between NL1 and NL2 is $98.53 \pm 0.18\%$. b, Left: Grouping of NL2 and NL3. Right: CC versus the relative phase ϕ_C when NL1 is blocked. The interference visibility obtained between NL2 and NL3 is $98.68 \pm 0.17\%$. The data are fitted with a sinusoidal curve. Errors are determined by assuming Poissonian counting statistics.



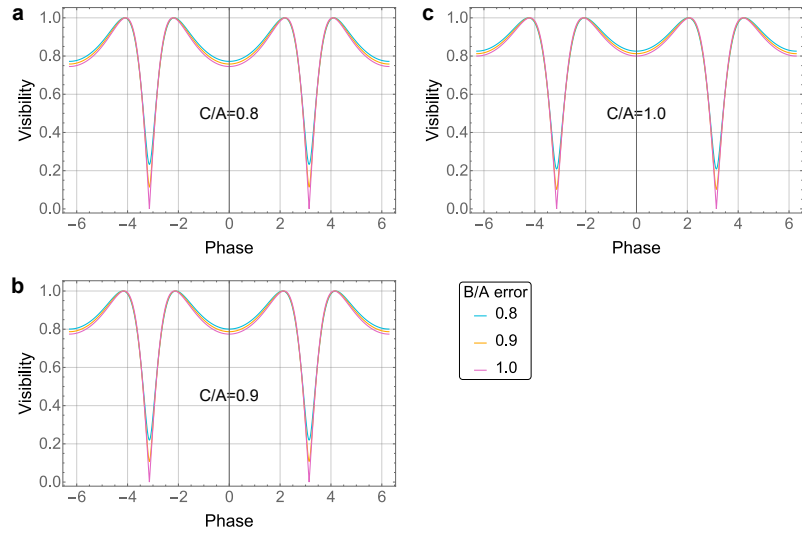
Supplementary Figure 9: a, Angle distribution of the SPDC photons versus the wavelength at different crystal temperatures. This is an ideal case. Normally, the central wavelength of the band-pass filter is not the same as the degenerate wavelength of the SPDC photons. In addition, the photons at 0° angle are not within the bandwidth of the filter. Therefore, we usually collect photons located at the rings filtered by the band-pass filter. b-g, Variation of the SPDC beam spot when changing the crystal temperature. In the experiment, the crystal temperature is optimised around 30°C .



Supplementary Figure 10: Count rate versus the phase ϕ_C (a) and phase ϕ_A (b). For comparison, the experimental counts are normalised with respect to the corresponding theoretical maximum.



Supplementary Figure 11: Visibility degradation caused by three different kinds of alignment errors. a, Schematic of the three errors. b, Visibility versus longitudinal error. c, Visibility versus transverse error. d, Visibility versus the tilt error.



Supplementary Figure 12: Visibility deviation due to the photon yield imbalance of the three crystals. a, b and c are for the different imbalance ratios C/A between NL3 and NL1. The three lines in each figure correspond to the different imbalance ratios $B/A = 0.8, 0.9, 1.0$ between NL2 and NL1, as shown in the legend. Here, the abscissa is the phase ϕ_A . The results are the same for phase ϕ_C .